Performance of Ti-15Mo alloy obtained by powder metallurgy route weakly alloyed with Fe/Cr elements

Mariana Correa Rossi [a*], Patrícia López Navarro[a], Angel Vicente Escuder [a], Vicente Amigó Borrás [a], and Emílio Francisco Segovia López[a]

[a] Universidad Politécnica de Valencia, Instituto de Tecnología de Materiales. Camino de Vera s/n, 46022 Valencia, España.

(* correspondence author:mrncorrea90@gmail.com)

Abstract

Ti-15Mo alloy can be an excellent choice as a biomaterial for prostheses. This is due to the combination of good mechanical properties and biocompatibility. The Mo is a stabilizing element of the β phase, which provides a smaller elastic modulus, reducing the risk of stress shielding that induces bone resorption. The present work shows the effect of minor additions of Fe or Cr on flexural fracture toughness in Ti-15Mo alloys obtained by Powder Metallurgy. The electrochemical results indicated that the Ti-15Mo-1Cr, showed greater resistance to corrosion, related to lower β grain size, less porosity content compared to the other conditions. As the Ti-15Mo-1Fe and Ti-15Mo-3Fe presented more porosity in their microstructure, the saline composition inside the pores is different in concentration and thus makes diffusion difficult compared to other regular and more homogeneous zones. Besides, was verified the effect of the large grain size that decrease the corrosion resistance of the Ti-15Mo-3Cr, demonstrated two influences in the corrosion resistance, porosity and grain size. Toughness decreases with the addition of both elements, more pronounced with Fe than Cr. It is related with lower densification, higher porosity and greater proportion of phase α in grain boundary due to the higher resistance of diffusion of Mo in Ti when Fe is present, which leads to failure by brittle fracture at lower shear stresses.

KEY−WORDS: Biomaterial – Fracture – Molybdenum – Shear– Titanium – Toughness

1. INTRODUCTION

At present, the market request for biomaterials is very high, due to different needs as related to the increase life expectance of world population and traffic accidents [1]. The uses of biomaterials in medical applications includes several areas: orthopedics, cardiovascular surgery, ophthalmology, dentistry, urology, aesthetic surgery, neurology, suture material for wound healing, and controlled release drug delivery systems [2]. In this sense, is very important to develop new materials enhancing the mechanical properties, biocompatibility, and long-term viability as an implant material. Fundamental requirements are that an implant should have stiffness, strength, fracture toughness, wear resistance, fatigue strength and corrosion resistance [3-8] and surface attractive for the cells [9]. In this sense, their properties depend on the microstructure, of the metallic materials and differs depending on the amount of α or β stabilizing elements added to them. Ti-based alloys are grouped into α-type, (α + β)-type, and β-type alloys. Alloying the pure titanium with β-elements leads to the widening of the β-phase domain, as well as the improvement of the biomechanical properties already proved in the literature [10-12]. Molybdenum (Mo) is an element with a lower degree of toxicity, and moreover, is a β-stabilizing element [13]. Studies in this field have highlighted that Ti alloyed with Mo in different percentages such as 15%–20% can decrease the elastic modulus leading to adequate mechanical properties close to bone tissue [14,15]. The Ti-15Mo alloy, it is already standardized for its forged state as ASTM F 2066 or UNS R58150. First works developed with Ti-Mo system, showed an elastic modulus between 70-80 GPa; closer to bone tissue (10-30 GPa), reducing the risk of stress shielding that induces bone resorption and/failure of the prosthesis purpose [3]. In this respect, it can be an excellent choice as a biomaterial for prosthetics due to the combination of good mechanical properties and biocompatibility. The fabrication of these kind of biomedical devices, powder metallurgy as an alternative method to casting and forging makes it possible to obtain pieces with dimensions more adjusted to those of the design, homogeneity of microstructure and composition, and adequate porosity that benefits osseointegration [16-18]. For a given Ti alloy composition, a well-known and useful parameter for characterizing the β-phase stability is the Mo equivalency (Mo_{Eq}). This quantity is a combined measure of the effects of β, α and neutral elements contained in a Ti alloy on the β phase stability [19-21]. It uses Mo as an arbitrarily chosen baseline and normalizes other elements to an equivalent Mo value. Mo equivalent theory was used to choose the concentration of the alloying elements to stabilize the β phase. So, as Mo is one of the main β stabilizing elements and, from 10% by weight, this phase is already reached [15]. Thus, an equation was arrived at that relates the equivalent percentage of Mo to other elements, indicators of β phase stabilization.

$$[Mo]eq = [Mo] + \frac{[Cr]}{0.63} + \frac{[Fe]}{0.35} \quad (1)$$

where [Mo], [Cr] and [Fe] is the concentration in percentage by weight of the referring element. Further is a strong β-stabilizer and is regarded as the most suitable β-stabilizer element because it is able to stabilize β-phase in low solute concentration. This is important because it is a refractory metal with a high melting point (2623 °C). So, the addition of this element to Ti increases the melting point making the processing of the material more difficult, provides low elastic modulus which is interesting by also low flexural strength [22].

In order to improve the strength, elements such as Fe and Cr also contribute to the stabilization of the β phase of Ti [23,24]. Some studies report the loss of ductility of Ti in the presence of Mo, Cr, or Fe [25-28] and some information obtained from the tensile or bending curves could be applied to characterize the tough behavior of the alloy, but it is not usually reported in the literature. There are also no studies in which shear stress is determined as an indicator of mechanical behavior when testing powder metallurgical materials in bending under a short beam configuration. So, the present work shows the effect of minor additions of Fe or Cr on the electrochemical resistance and flexural fracture toughness of Ti-15Mo alloys obtained by sintering an elemental powder mixture (conventional powder metallurgy), as well as the shear failure stress associated with ductile brittle behavior of these alloys.

2. MATERIALS AND METHODS

2.1. PROCESSING SAMPLES BY PM

Alloys studied in the present work obey the denomination Ti-15Mo-X, where X represents the nominal content of Fe or Cr: 0, 1 and 3%; which constitutes respectively Mo equivalent by weight of 15.0 %, 16.6 %, 19.76 %, 17.85 % and 23.6 % [29]. Materials have been formulated from powder of: Ti with a particle diameter (pd) <44 μm, minimum purity (m.p) 99.7%, supplied Phelly; Mo of pd <4 μm, m.p 99.9%, supplied by Atlantic EE; Fe pd <38 μm, m.p 99.9%, supplied by Höganas; Cr of pd <44 μm, m.p 99.8%, supplied by α-Aesar. Conventional powder metallurgical manufacturing procedure followed includes the following stages: elemental blending of powders (blending elements) for 30 min at 50 rpm, 600 MPa compaction pressure and consolidation in 2 phases in a high vacuum furnace (P $<10^{-4}$ mbar) as following: (I) heating at 15 ºC/min up to 800 ºC kept for 30 min, (II) heating at 10 ºC/min up to 1250 ºC kept for 2 h, concluding with cooling at 10 ºC/min until room temperature. Dimensions of the sintered specimens were: length 28.2 ± 0.2 mm, width 11.5 ± 0.2 mm and thickness 5.5 ± 0.1 mm.

2.2 PHYSICAL CHARACTERIZATION

Physical properties such as density (D), relative density (R_D) and porosity (P) have been determined under the UNE-EN-ISO 2738: 2000 standard in 3 samples of each alloy, with different content of Fe and Cr. The porosity was also determined by image analysis on 10 different internal areas of each sample using a Nikon LV-100 microscope, equipped with the Nikon Nis-Elements AR analyzer program.

2.3 STRUCTURAL AND MICROSTRUCTURAL PROPERTIES OF Ti-Mo-X

Fractographic study was carried out on a Zeiss U55 field emission scanning electron microscope, also allowing to obtain information about the homogeneity of the alloys. To characterize more precisely the microstructure, like the grains and the phase quantifications was used electron backscattered diffraction (EBSD) with a scanning electron microscope (Zeiss Auriga Compact operating at 20 kV equipped with an Aztec HKL Max System (Oxford Instruments Ltda) under an acceleration voltage of 20 kV with a step size of 1 μm, selecting two possible phases to be analyzed, β-Ti and α-Ti were made by EBSD backscattered electron diffraction performed with a Zeiss Auriga Compact scanning electron microscope.

2.4 MECHANICAL EVALUATION AND FRACTURE OF THE Ti-15Mo-X

Mechanical properties of the samples were obtained by the ultrasound tests. From these tests was possible to determine the elastic modulus (E), Poisson's ratio (ν), and shear modulus (G). First the measurement of the longitudinal and transverse propagation velocity of waves within rectangular specimens were analyzed. The 3-point bending tests were carried out on a Shimadzu AG-100KN universal testing machine, in accordance with the UNE-EN-ISO 3325: 2000 standard. A total of five specimens of each alloy have been tested. The toughness was determined as breaking energy W_O from the area under the load-deflection curves (F-d), or as specific breaking energy W_V from the area under the stress-strain curves (R-ε).

The test configuration is under short beam, in which the length relationship between supports (L) and specimen thickness (h) was equal to 4, it being possible to calculate the apparent shear stress (S) by bending at the instant in which the breaking stress (R_B) were obtained by the follow equations:

$$R_B = \frac{3\,F\,L}{2b\,h^2} \quad (2)$$

$$S = \frac{3F}{4\,b\,h} \quad (3)$$

2.5 INFLUENCE OF Fe AND Cr CONTENT ON THE CORROSION RESISTANCE OF Ti-15Mo ALLOY

Potentiodynamic corrosion tests were carried out at 37ºC in the same solution using a surface area of 0.785 cm^2 of each sample as a work electrode, Ag/AgCl, 3M KCl as a reference electrode in a Metrohm potentiostat (model PGSTAT204). Tafel´s slope cathodic (β_c) and anodic (β_a), corrosion current densities (i_{corr}) and Potential corrosion (E_{corr}) were estimated from Tafel plots. Three measurements of all the tests were performed at a scan rate of 2 mV/s. In order to estimate the corrosion rate (C_r) the follow equation was used:

$$C_r = 3.15^{11} i_{corr} \frac{Mwalloy}{nalloy\ F} dalloy^{-1} \ (4)$$

Where, M_{walloy} is the atomic mass of the titanium, n is the valence electrons of the titanium, molybdenum, chromium and iron, and F is the Faraday's constant. Finally, Electrochemical Impedance Spectroscopy (EIS) was obtained with a FRA32M module combined with the potentiometer in the same solution at a frequency range from 100 MHz to 5 mHz and a signal amplitude of 10 mV at OCP for 1800 s. Impedance data were analyzed by the Zview software and fitted to simple porous layer equivalent circuits.

3. RESULTS AND DISCUSSION

3.1 LOW CONTENT OF Cr AND Fe IN Ti-15Mo ALLOY PRESENT OPPOSITE MICROSTRUCTURE FORMATION

The microstructures obtained from PM of Ti-15Mo alloy with and without Fe and Cr content are represented in figure 1a-e. The Ti-15Mo alloy indicated in figure 1a is formed by a micropores microstructure, which is normally found in samples fabricated by PM, that depending on the particle size, chemical composition of the alloy and also the compaction pressure used. Further Mo is a β stabilizer element, characterized as refractory feature which is difficult its sintering. In figure 1b-c also can be seen the same microstructure, nonetheless it seems to be less porous with addition of Cr 1 or 3 wt %. For the samples sintered with Fe 1 or 3 wt%, the microstructure was formed by micro and microporosity, indicating less homogeneity compared to Cr content. In table 1 clearly it is note the influence of Cr and Fe in the porosity formation in Ti-15Mo alloy. Comparing to the control sample (Ti-15Mo), there was a decreasing of 36% and 72% in porosity (3.2 % and 1.4 % of porosity-Table 1) with addition of Cr (1 and 3 wt%) while with addition of Fe (1 and 3 wt%) there was an increasing in 18% and 22% of porosity (5.9 % and 6.1 % of porosity-Table 1). The β stabilizers Cr and Fe elements seems to promote opposite effects on the microstructure, which is can be related with his physical features.

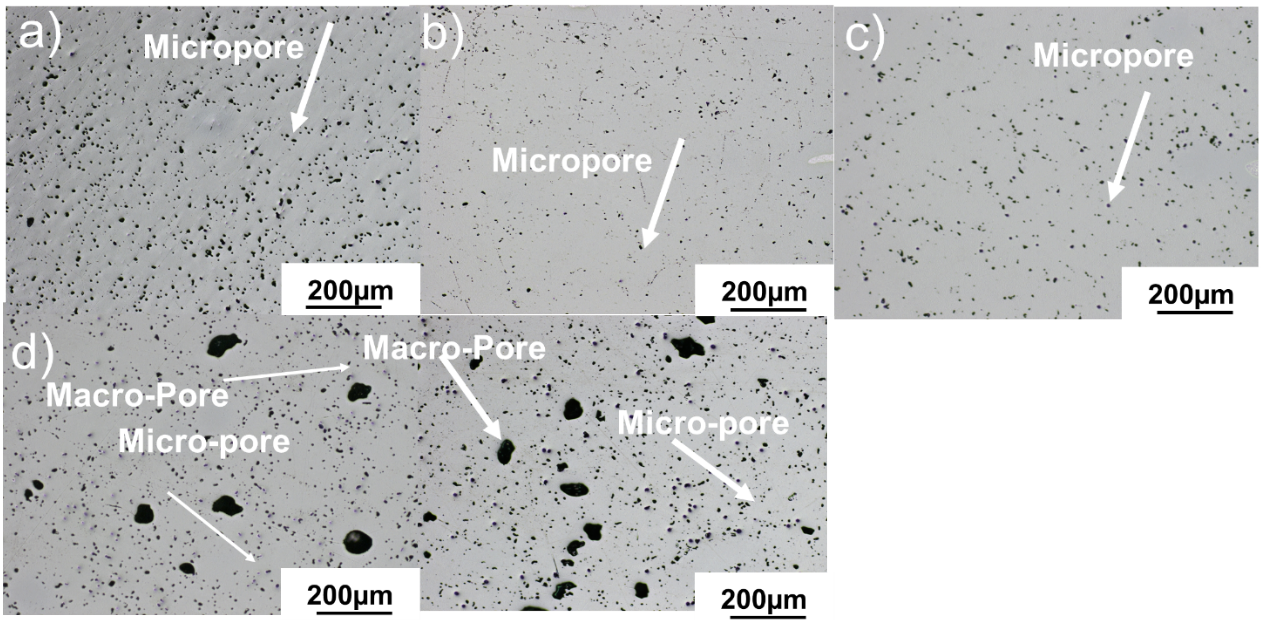

Figure 1. SEM of Ti-Mo-X (%) system. a) SEM of Ti-15Mo alloy b) SEM of Ti-15Mo-1Cr, c) SEM of Ti-15Mo-3Cr, d) SEM of Ti-15Mo-1Fe, e) SEM of Ti-15Mo-3Fe.

Table 1. Physical characteristics of Ti-15Mo -X alloys

X (%) [a]	**D (g/cm^3)**	**D_R (%)**	**P (%)**	**P_O (%)**	**D_G (µm)**
0	4.73 ± 0.02	96.0 ± 0.4	4.0 ± 0.3	5.0 ± 0.3	24
1% Fe	4.71 ± 0.02	95.3 ± 0.6	4.7 ± 0.4	5.9 ± 0.3	28
3% Fe	4.69 ± 0.02	94.0 ± 0.5	6.0 ± 0.5	6.1 ± 0.4	38
1% Cr	4.71 ± 0.01	95.4 ± 0.3	4.6 ± 0.3	3.2 ± 0.3	23
3% Cr	4.75 ± 0.04	95.6 ± 0.6	4.4 ± 0.6	1.4 ± 0.4	26

3.2. EFFECT OF THE ADDITION OF Fe OR Cr ON THE PHASE FORMATION OF Ti-15Mo-X ALLOYS

Details of the microstructure of Ti-15Mo containing 1 or 3 wt% Cr and Fe are represented in figure 2. The Ti-15Mo-1Cr and Ti-15Mo-3Cr alloys are indicated in figure 2a-b. Both alloys present the same microstructure formed majority by large β equiaxed grains (18.58±16.14 µm for

Ti-15Mo-1Cr and 24.21 μm ± 16.4 μm for Ti-15Mo-3Cr), and around the grain boundaries the presence of needles α-phase grains (3.50 μm ± 1.29 μm for Ti-15Mo-1Cr and 3.18 μm ± 0.89 μm Ti-15Mo-3Cr) in dark contrast. It is possible to note that the presence of α decrease with the increase of the Cr content and the β grain size increases when increase the Cr content. The same microstructure was found in the Ti-15Mo-1Fe and Ti-15Mo-3Fe indicated in figure 2 c-d, which are also formed by large β grains (10.85±8.21 μm for Ti-15Mo-1Fe and 18.44 μm ± 17.01 μm for Ti-15Mo-3Fe) microstructures and grain boundaries well defined with presence of α needles at the grain boundaries (4.41±2.8 μm for Ti-15Mo-1Fe and 2.44 μm ± 1.09 μm for Ti-15Mo-3Fe). The presence of the α (PDF: 44-1294) and β (PDF: 44-1288) phase was also confirmed by X-ray diffraction measurements, in figure 3. The DRX patterns of all the samples, also in control sample (Ti-15Mo) are structured under 2 phases, as was showed in figure 2, being α (compacted hexagonal) and β (body centered cubic), as well as their crystallographic planes. From the XRD patterns it is clearly noted an increase in β phase represented by the (110), (200), (211) and (220) planes. The suppress of α phase can be mainly noted in the XRD patterns of the Ti-15Mo-3Fe and Ti-15Mo-3Cr samples where the $(100)_{\alpha}$, $(101)_{\alpha}$, $(102)_{\alpha}$, $(110)_{\alpha}$, $(112)_{\alpha}$ and $(201)_{\alpha}$ planes show higher decrease in its intensity compared to samples with less β stabilizer elements content. Phase quantification was obtained through Maud and SearchMatch softwares and their values are indicated in table 2. By this result can be say that Cr content present higher β stabilizer effect than the Fe. Moreover, it is note an antagonic effect of Fe 3 wt %, where the α phase increase.

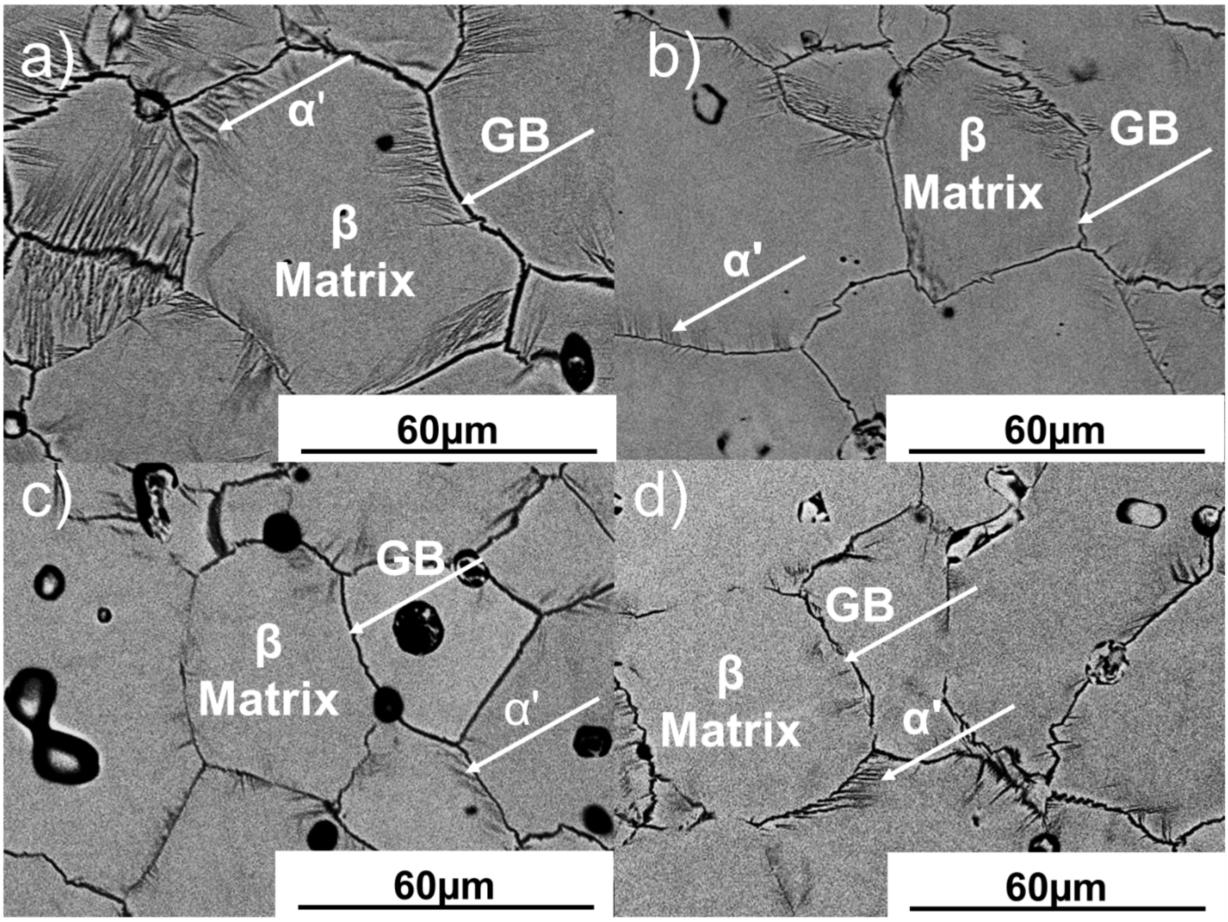

Figure 2. Microstructure of the Ti-15Mo-X alloys obtained by FESEM. A greater presence of β phase is appreciated with the Cr content.

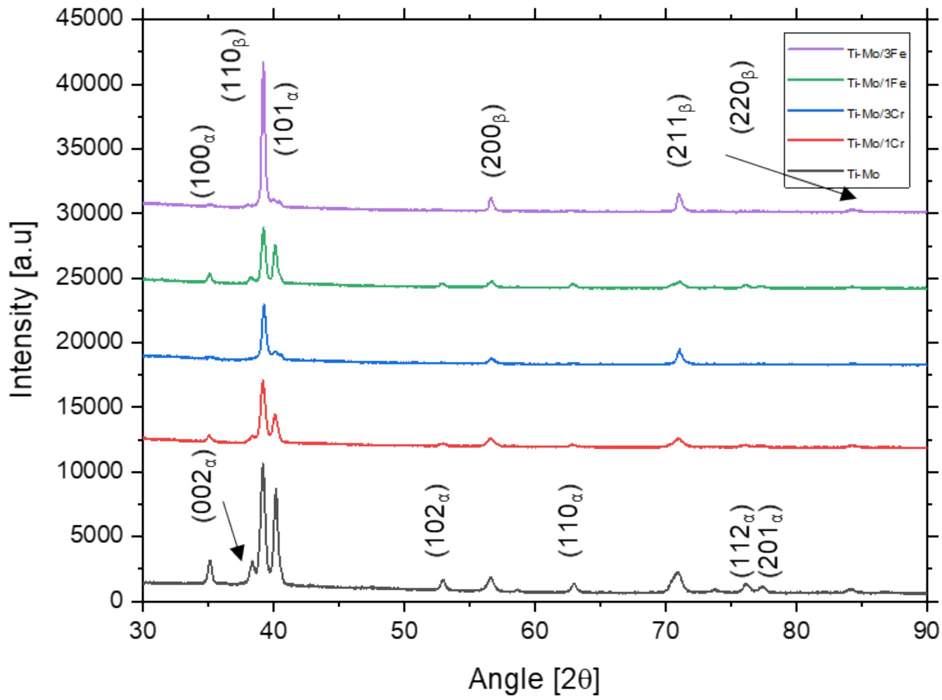

Figure 3. XRD pattern of Ti-Mo-X (%).

Table 2. Phase content in different Ti-Mo-X (%) alloys.

X (%)	Phase β (%)	Phase α (%)
0	95.2	2.7
1% Fe	94.6	3.4
3% Fe	93.4	2.3
1% Cr	96.1	3.2
3% Cr	96.4	2.8

3.3 CORROSION RESISTANCE INFLUENCED BY THE β STABILIZER ELEMENTS IN Ti-15Mo-X ALLOYS

The OCP variation as a function of time for Ti-15Mo and Ti-15Mo-(Cr/Fe) are represented in figure 4a-d. For the Ti-15Mo samples (Figure 4a), the potential increases exponentially until it reaches a steady state because of the passive film thickening at the surface, with a potential of 0.199V. For Ti-15Mo-1Cr and Ti-15Mo-1Fe indicated in figure 6b and c it is note the potential also increase exponentially as the first one, however the stability of the passive film is not adequate, where can see some regions in the curve related to the break of it. For the figure 6c, this feature is less intense. For the Ti-15Mo-3Cr represented in figure 6d there is no evidence the loss of passive film, also the potential increase until reach at -0.152 V. In figure 6e where is indicated the OCP for Ti-15Mo-3Fe, the potential increase exponentially until it reaches 0.273 V and there was not a loss of passive film. In this sense, the 15Mo weakly alloyed with Cr present a passive layer more stable than with the low content of Fe.

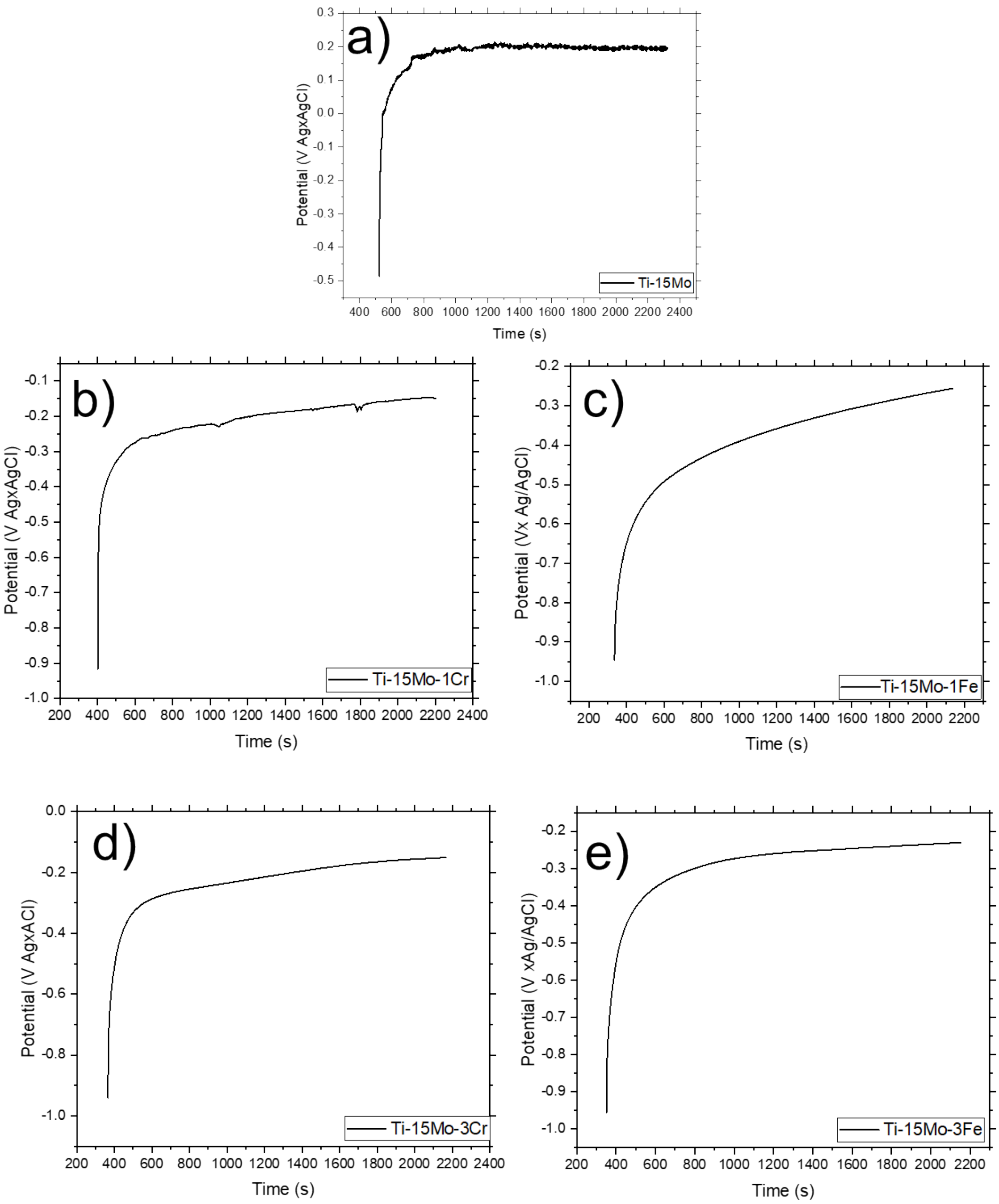

Figure 4. Open circuit potential (OCP) as a function of time, for the samples of alloys of Ti–15Mo–X system.

Potentiodynamic polarization curves obtained for the Ti-15Mo-X alloy in Ringer Hartmann's solution at 37ºC are shown in figure 5a-d. As seen, after the active dissolution of Ti-15Mo (Figure 5a) it exhibits a large passive plateau (0.873 to 2.280 V vs. Ag/AgCl) characterized by passive current density in the order of 10^{-4} A/cm^2. The current density increases at potential around 0.727 V likely because of the oxygen evolution reaction at the oxide surface.

At this point the current densities started to decreases until the transpassivation occur indicated by the arrows. For figure 5b-c are indicated the PPCs of the Ti-15Mo-(1/3Cr). It is note that Ti-15Mo-1Cr present a large passive plateau and there is no evidence of transpassivation phenomenon whereas for the Ti-15Mo-3Cr exhibit a narrow passive plateau at -0.54 V by passive current densities in the order of 10^{-5}A/cm^2. Then the transpassivation mechanism occur indicated by the arrow and the current density decrease. For 1 and 3 Fe wt% the PPCs are indicated in the Figure 5d-e, where for Ti-15Mo-1Fe exhibit a good large passive plateau characterized by passive current densities in the order of 10^{-3}. From this point the current density increases at potentials around 1.29 V likely also because of the oxygen evolution reaction at the oxide surface. For Ti-15Mo-3Fe exhibit a large passive plateau characterized by passive current. The current density increases at potential around 1.334 V likely because of the oxygen evolution reaction at the oxide surface. At this point the current densities started to decreases until the transpassivation occur indicated by the arrows quite similar to the Ti-15Mo.

It possible is caused by the electrochemical dissolution of alloy surface and the next formation of nonstoichiometric titanium oxides which slow dissolution process:

$$Ti^{3+} + xH_2O \rightarrow TiO_x + 2xH^+ + (2x\text{-}3)e^- \quad (4)$$

At potentials 0.04-1.16 V vs. Ag/AgCl of PPCs for Ti-15Mo-3Cr there is the transpassivation of surface, caused by forming of unstable titanium oxychloride $TiOxCl_2$ which is oxidized to titanium dioxide, that causes the existence of the passive region at potentials 3 V Ag x AgCl.

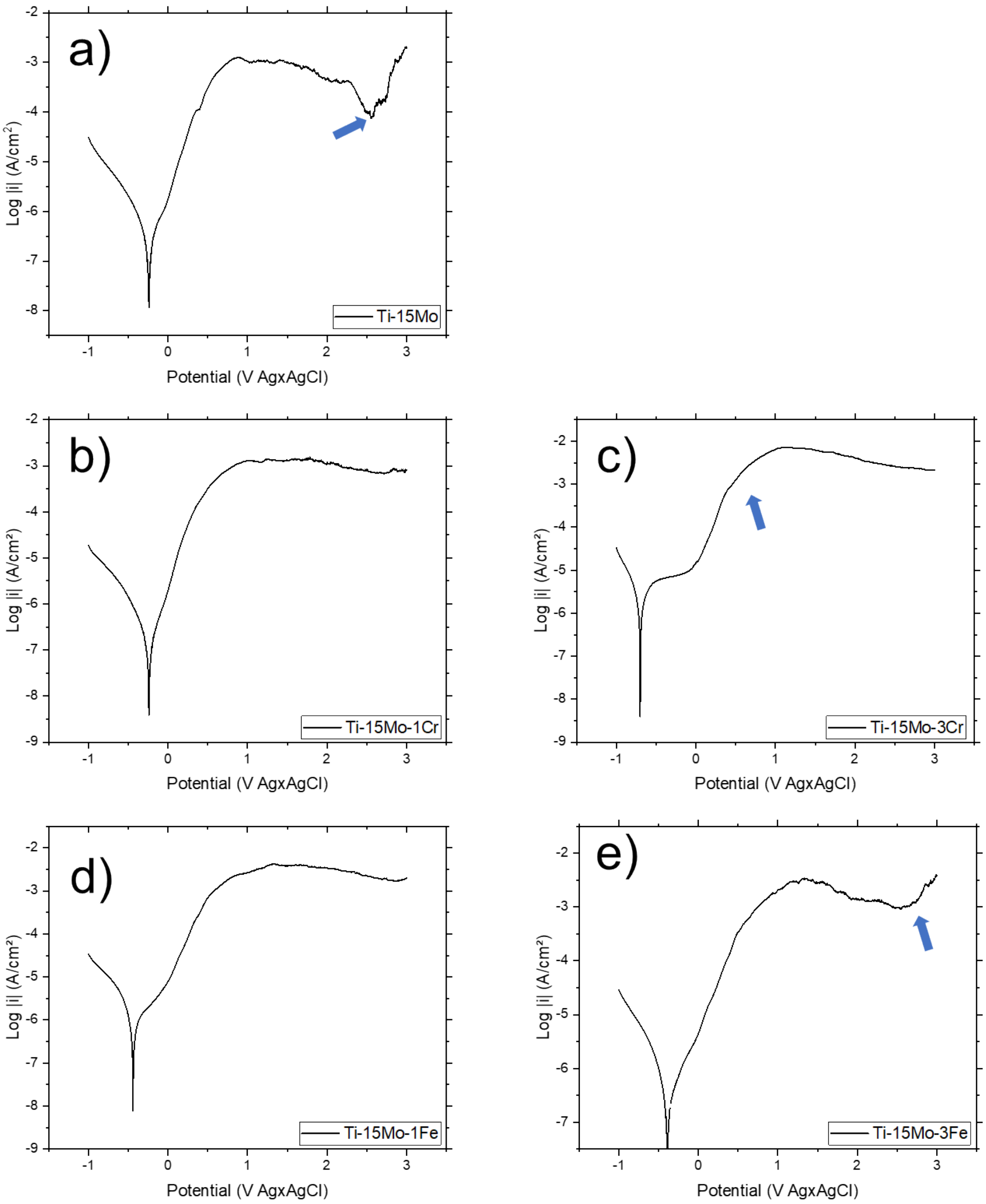

Figure 5. Potentiodynamic polarization curves (PPCs) curves of Ti-15Mo-X alloys obtained in contact to the Ringer Hartmann's solution at 37ºC.

In table 3 are presented the instantaneous corrosion parameters in the same physiological environment that the OCP and PPCs. Corrosion potential (E_{corr}) measured relative to the potential of the Ag/AgCl reference electrode, is the potential at which the oxidation-reduction reactions on the alloy surface are at equilibrium; the rate of the oxidation reaction is equal to the rate of the reduction reaction, and the total current intensity is zero. Increasing the potential to more positive values increase the rate of the oxidation reaction, while the potential shift to negative values is reduced by the oxidation process and the metal passes. It can be seen that the presence of 1 Cr appears to decrease the corrosion rate compared to the presence of 1 Fe and also compared to Ti-15Mo, which is the sample control. Samples obtained with 3Cr present higher rate corrosion compared to the others, followed by 3Fe. This significative difference between the samples with low betagenic element content can be explained by the presence of porosity and the grain size in their microstructure. Ti-15Mo-1Cr present β grain size about 18.6 μm, which has showed low corrosion rate, followed by Ti-15Mo-1Fe and Ti-15Mo that presented 10.8 μm and 19.5 μm of β grain size while for Ti-15Mo-3Cr indicated higher corrosion rate with β grain size about 24.2 μm followed of Ti-15Mo-3Fe with 18.4 μm which has similar grain size of Ti-15Mo-1Cr but presented more porosity in it is microstructure. The "corrosive" product of these alloys is mainly TiO_2, which is insoluble and adherent to the surface of the alloy. The oxide layer on the surface protects the alloy against the aggressive action of electrolyte medium. Considering the grain sizes of β grains and the porosity formed, this it can be concluded that in the physiological environment used in this work, β-titanium-based alloys with 1 Cr present a fast passivation process and low corrosion rate. Under these conditions the variable corrosion rate is actually passivation rate. The value of Cr and Fe concentrations are important for corrosion studies. The low concentrations of Cr and Fe have a significant influence on the corrosion parameters, thus, the corrosion resistance for Ti-15Mo-1Cr> Ti-15Mo-1Fe> Ti-15Mo> Ti-15Mo-3Fe> Ti-15Mo-3Cr.

Table 3. Kinetics parameters obtained from PPCs.

	i_{corr} (μA/cm^2)	E_{corr} (V)	R_p (kΩ/cm^2)	C_r (nm/year)
Ti15-Mo	0.24 ± 0.02	-0.47 ± 0.36	106 ± 10	22
Ti15Mo1Cr	0.08 ± 0.2	-0.22 ± 0.02	338 ± 92	7

Ti15Mo3Cr	0.71 ± 0.08	-0.60 ± 0.15	36 ± 5	65
Ti15Mo1Fe	0.22 ± 0.12	-0.36 ± 0.11	130 ± 67	21
Ti15Mo3Fe	0.37 ± 0.36	-0.48 ± 0.12	136 ± 134	34

As can be seen in the Nyquist diagrams, at the corrosion potential the radius of the semicircle is very small, which indicates a low polarization resistance on what is the same, a low resistance to corrosion because on the material begins to form a passive layer, the resistance to form a passive layer. At the potential increases, the resistance to polarization and implicitly the resistance to corrosion increases. In comparison with the diameter of the circle arc of Ti-15Mo, it can be found that the Ti-15Mo-1Cr showed a much large diameter, also when it compared to the Ti-15Mo-3Cr. For the Ti-15Mo-1Fe the diameter of the circle arc is quite similar to the Ti-15Mo, while Ti-15Mo-3Fe presented small diameter of the circle arc compared to all of them.

All values of circuit arc elements for the alloys are listed in table 4. The circuit elements values for the solutions resistance (Rs) are about the same order.

The true capacitance values were within a range of 0.284-1.4 10^{-5} F/cm^2, and the values of n were in the range of 0.78-0.89, which indicated a non-ideal capacitance interface for Ti-15Mo-3Fe.

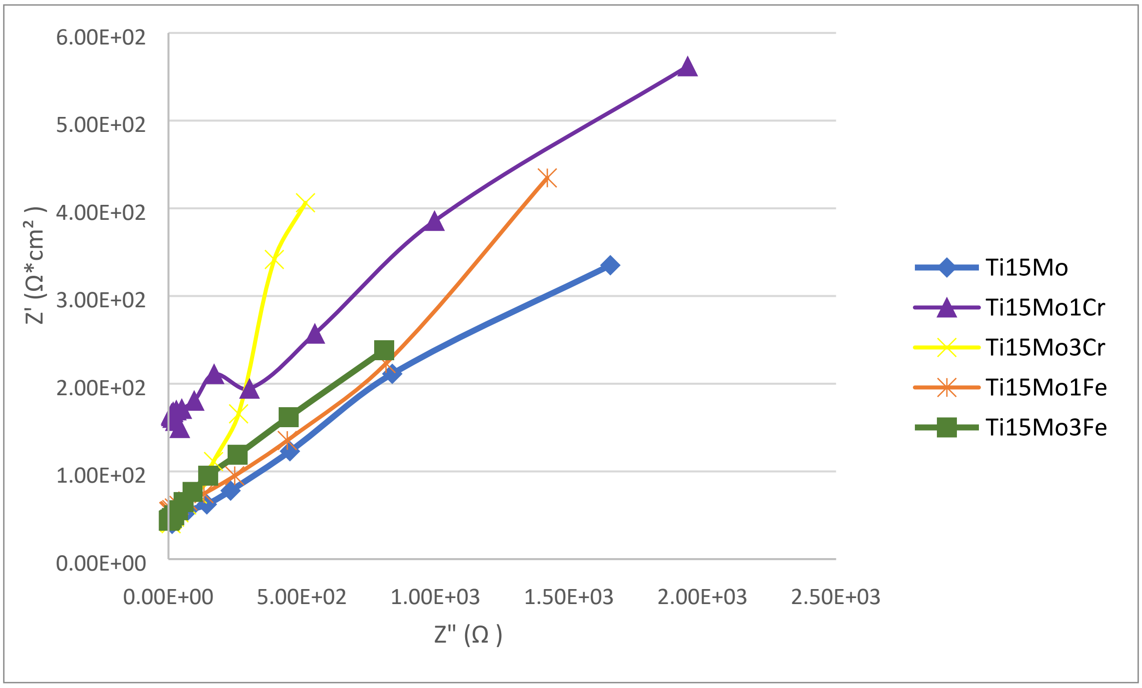

Figure 6. Typical Nyquist diagram for the Ti-15Mo-X alloys.

Table 4. Parameters calculated from the electrochemical impedance spectroscopy (EIS) measurements.

	Chi-Sqr (10^{-3})	Rs (Ωcm^2)	CPEdl-T ($10^{-5}F/cm^2$)	N	Rct ($K\Omega cm^2$)
Ti15-Mo	0.24	59.07±12.45	5.31±0.67	0.88±0.01	6.87 ±2.64
Ti15Mo1Cr	0.88	107.93±57.61	3.41±0.56	0.89±0.02	24.62±4.14
Ti15Mo3Cr	0.37	64.40±41.24	6.20±2.11	0.85±0.04	1.40±0.40
Ti15Mo1Fe	0.05	52.10±3.25	5.82±1.44	0.85±0.04	5.91±3.73
Ti15Mo3Fe	1.80	43.20±1.41	12.80±1.98	0.78±0.02	1.71±0.35

3.4. ELASTIC BEHAVIOR OF Ti-15Mo-X

The elastic properties obtained by ultrasound measurements are shown in table 5. For each sample, its respective values of elastic modulus (E), shear modulus (G) and Poisson constant (ν) are indicated. The E found for the Ti-15Mo alloy, being higher than the values found in the works by Ho et al, 1999 and Mohamed et al., 2014 (71 GPa and 78GPa) with a fully β structure [15,30]. The G found was 37.8 GPa, very close to CP-Ti studied in the work of Zhao et al., 2021 [31]. In addition to the search for adequate values of elastic modulus in the biomedical field, the study and the effect of the microstructure on G is also of great relevance in designating the ductility of β-Ti alloys. To the addition of Fe 1 wt% the elastic properties are not changed, nonetheless with 3 wt% the E as well as G drop by 5.3% and 4.5% %. However, for the Ti-15Mo alloys with 1 or 3 wt% of Cr, the elastic properties had very little decrease, showing no difference between 1 or 3 wt% of Cr content. Regarding ν, the values found are very similar to those in the literature (0.33), while G is lower than those of alloys obtained by forging (52 GPa). The G in general is lesser to forging alloys due to the porosity found, as previously observed, in the microstructures of Ti-15Mo-1/3Fe alloys. In the work by Xu et al. 2018 reported that the Ti-10Mo alloy with 2.8% porosity had 66GPa of E with full β microstructure. Also, in the work of Martins et al. 2014 samples were obtained Ti-15Mo, between 75-100GPa of E, in which they presented 0.25% of interstitial oxygen, related to the presence of α' phase in a mostly β structure (73-98%) as well as, Yan et al. 2014 obtained E between 105-110 GPa for Ti-15Mo alloys with mostly β microstructure, with small α+α´ phase content [33]. The Ti-15Mo-X alloys studied in this work, with higher Mo content and higher porosity, seem to be affected by the hardened phases which are present at the beginning of the slow cooling steps, which do not significantly contribute to the significant reduction of the values and consequently for the G values.

Table 5. Elastic properties of alloys Ti - 15Mo - X

X (%)	**E (GPa)**	**G (GPa)**	**ν**
0	100.5 ± 0.4	37.8 ± 0.2	0.331 ± 0.001
1% Fe	100.2 ± 0.5	37.7 ± 0.2	0.328 ± 0.002
3% Fe	95.2 ± 1.2	36.1 ± 0.5	0.318 ± 0.002

1% Cr	99.2 ± 0.5	37.4 ± 0.2	0.327 ± 0.001
3% Cr	99.0 ± 0.9	37.3 ± 0.4	0.327 ± 0.001

3.5. TOUGH AND STRENGTH BEHAVIOR OF Ti-15Mo-X

The toughness of the material in terms of breaking energy under the load-deflection curve (W_O) and energy per unit volume (W_V) under the stress-strain curve is presented in table 6. The results showed high flexural strength R_B (1530 MPa), as indicated by Hsu et al [34] and Ho et al. 1999 [15] when alloying Ti with Mo. The addition of Fe or Cr to the base alloy Ti-15Mo decreases R_B mainly for Ti-15Mo-(1 or 3 Fe wt%). Therefore, the shear failure stress S at the moment of failure also decreases and this effect is more pronounced with Fe than with Cr, consequently, resulting in a loss of toughness. While for the Ti-15Mo alloy with 3 Fe wt% presented 4.7 J and 29 J/cm^3, with losses up to 70% in W_O and W_V, confirming the loss of ductility due to the effect of Fe in Ti-Mo alloys [35,36].

In the case of Ti-15Mo-3Cr, the toughness also decreases, but to a lesser degree: 3.2 J (34%) and 20 J/cm^3 (31%).

The fractographic analyses of the base alloy Ti-15Mo, in figure 7, indicates a rough fracture, typical of a ductile failure mechanism which exhibits substantial plastic deformation prior to failure. Ductile fracture mechanism is usually slow, and a large amount of plastic flow is concentrated near the fracture faces. Also occurs after yield stress, whereas brittle failure is fast and can occur at lowest stress levels than a ductile failure. Area under the stress strain curve represents the absorbed energy before failure and during the ductile failure the energy required is higher than the brittle failure.

This justifies the higher toughness of the material (4.7 J and 29 J / cm^3) since it can withstand higher shear stress (198 MPa). The addition of 3wt% of Fe results in a faceted breakage characteristic of a brittle cleavage fracture mechanism. The toughness drops dramatically to 1.4 J and 9 J/cm^3; since the capability to withstand shear stresses at the moment of maximum load is much lower (96 MPa). In the Ti-15Mo-3Cr alloy, a lower incidence of cleavage is observed, combined with the roughness of the ductile mechanism. The toughness for 3 wt% Cr decreases to 3.2 J and 20 J/cm^3, but to a lesser extent than with Fe additions. The shear stresses that the ternary alloys Ti-15Mo-Cr withstand at the instant of failure are lower than those of Ti-15Mo (171-164 MPa), but these remain higher than the corresponding Ti-15MoFe (155-96 MPa).

Loss of toughness is influenced by porosity, densification and microstructure. The addition of Fe decreases densification and increases porosity, as seen in table 1, more intensely with respect to Ti-15Mo and Ti-15MoCr alloys. The difficulty of diffusion of Mo in Ti is also a factor of embrittlement, producing alloys less dense and of greater porosity in the presence of Fe or Cr [37-39]. Densifications obtained with 15% Mo are higher than those reported by Wei et al. 2003 and Liu et al. 2006 [40,41]. In figure 1 shows black areas corresponding to the porosity derived from the higher Fe content that diffuses with some ease towards Ti, but not the opposite. The addition of Cr exhibits densification and porosity similar to that of Ti-15Mo. Cr produces synergistic effects in the diffusion mechanism between Mo and Ti, which would explain a more tenacious behavior than with Fe additions and a similar fractography with Ti-15Mo, even observing in some sporadic points an occasional lack of diffusion in the form of particles of Mo light gray color in the image corresponding to Ti-15Mo-3Cr (seen in figure 5c). The microstructure is mainly made up of β grains with the presence of α-phase needles at the edge of the grain, figures 3 and 4. Ebied et al. 2017 indicate the absence of ω phase in Ti-17Mo alloys [42]. Neither did Ho et al. 2008 report the existence of ω phase in casting alloys with Mo equal to or greater than 15% [43]. The β-phase content of the Ti-15Mo alloy is 95.2%, table 5, being 2.7% for the α-phase and 2.1% porosity. The addition of 1 and 3% Fe causes the β phase to decrease to 94.6 and 93.4% respectively, increasing the porosity to 4.3% due to the presence between 2.3 and 3.4% of α phase. The β phase remains slightly higher than 96% with Cr while the α phase content (2.8 to 3.2%) does not promote worse toughness since the porosity remains very low. These data confirm, on the one hand, the diffusion difficulties of Mo and Ti in the presence of Fe and the consequent loss of toughness; and on the other, the improvement of the diffusion between both in the presence of

Cr, contributing to a tenacious behavior closer to that of the Ti-15Mo alloy. The appearance of α phase in the form of needles at the grain edge hardens excessively, contributes to the brittleness of the material (Ivasishin et al., 2008; Min et al., 2010c; Esteban et al., 2011; Yan et al., 2014; Hsu et al., 2015; Xu et al., 2018) [34, 44-48] and the subsequent failure due to cleavage by exhibiting a lower tolerance to shear stress. On the other hand, the microstructure reveals that the mean diameter of the β grain is 24 μm in Ti-15Mo. Additions of Fe raise it to 38 μm, while with Cr they are close to that of Ti-15Mo (23-26 μm), remaining below those reported by Liu et al. (2003) and Liu et al. (2006) [41, 49]. The diffusion of Mo in Ti is carried out through the grain edge, which produces a beneficial effect on the refining of the β phase (Liu et al., 2003) [49]. A larger grain size contributes to an inhibition of densification and an increase in porosity [38,47], meaning a less tough behavior and a predisposition to brittle fracture. In this case, the synergy of Cr in the diffusion of Mo prevents the thickening of the grain and attenuates the brittle behavior.

Table 6. Strength and tough flexural characteristics of Ti - 15Mo - X alloys.

X (%)	R_B (MPa)	S (MPa)	W_O (J)	W_V (J/cm^3)
0	1530 ± 120	198 ± 16	4.7 ± 0.7	29 ± 4
1% Fe	1195 ± 100	155 ± 14	3.0 ± 0.4	19 ± 3
3% Fe	747 ± 71	96 ± 9	1.4 ± 0.2	9 ± 1
1% Cr	1329 ± 210	171 ± 27	3.5 ± 1.0	22 ± 7
3% Cr	1281 ± 137	164 ± 18	3.2 ± 0.6	20 ± 4

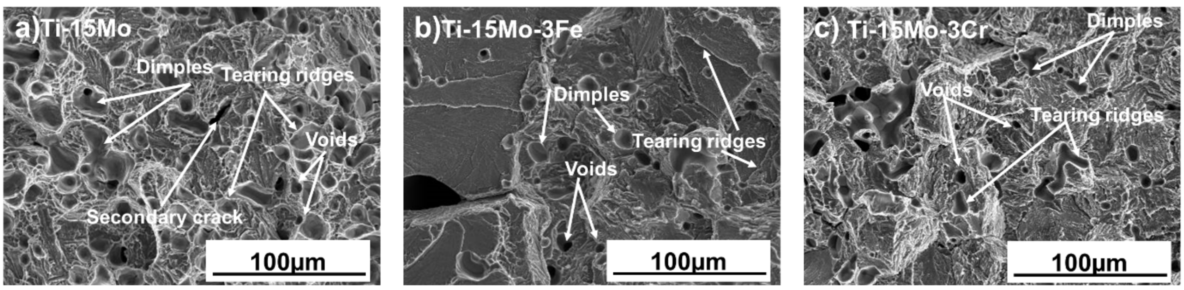

Figure 7. Fracture surface of Ti-15Mo-X alloys.

4. CONCLUSION

1. The Ti-15Mo alloy elaborated in this work presents high resistant properties: elastic, flexural and shear; in addition to being tough, due to its high densification, low porosity and mostly β microstructure, with the presence of α phase.

2. The addition of Fe (1-3%) to the Ti-15Mo alloy decreases the tough behavior to a greater degree than with Cr (1-3%), showing lower shear failure stress values and a more brittle fracture behavior. The Cr addition shows tougher fracture and similar to that of the base alloy Ti-15Mo.

3. The diffusion of Fe in Ti interferes with the diffusion of Mo, leading to higher porosity, lower densification, lower β-phase content, and larger grain size. The presence of α-phase needles at the grain edge justifies a higher value of elastic modulus in tensile and lower than that of shear.

4. The samples of Ti-15Mo, Ti-15Mo-3Cr, Ti-15Mo-1Fe and Ti-15Mo-3Fe showed greater resistance to corrosion, which may be due to the effect of the microstructure (larger β grain size, greater porosity), its elemental composition (difficulty in diffusing Mo in the Ti matrix when in the presence of Fe) in addition to the internal thickness-composition-strains discontinuity of the passive layer of TiO_2. Furthermore, the saline composition within the pores is different in concentration and thus makes diffusion difficult compared to other regular and more homogeneous zones.

ACKNOWLEDGMENT

The authors of this work thank the collaboration of the staff of the electron microscopy service of the Universitat Politècnica de València, as well as the financing received by the Ministerio Español de Ciencia, Innovación y Universidades (grant RTI2018-097810-B-I00).

REFERENCES

[1] Bataineh AB, Elarabi MS. Changing pattern and etiology of maxillofacial fractures during the civil uprising in Western Libya, Med. Oral Patol. Oral Cir. Bucal. 23; 2018. https://doi.org/10.4317/medoral.22268.

[2] Sandu AV, Baltatu MS, Nabialek M, Savin A, Vizureanu P. Characterization and Mechanical Proprieties of New TiMo Alloys Used for Medical Applications, Materials (Basel, Switzerland), 12; 2019. https://doi.org/10.3390/ma12182973.

[3] Niinomi M, Hattori T, Morikawa K, Kasuga T, Suzuki A, Fukui H, Niwa S. Development of Low Rigidity β-type Titanium Alloy for Biomedical Applications, Mater. Trans. 43; 2002. https://doi.org/10.2320/matertrans.43.2970.

[4] Amjad M, Badshah S, Rafique AF, Adil Khattak M, Khan RU, Abdullah Harasani WI. Mechanism of Fatigue Crack Growth in Biomedical Alloy Ti-27Nb, Materials (Basel, Switzerland). 13;2020. https://doi.org/10.3390/ma13102299.

[5] Zhang W, Liu Y, Wu H, Song M, Zhang T, Lan X, Yao T. Elastic modulus of phases in Ti–Mo alloys, Mater. Charact, 106; 2015. https://doi.org/10.1016/j.matchar.2015.06.008.

[6] Song Y, Xu DS, Yang R, Li D, Wu ZX, Guo ZX. Theoretical study of effects of alloying elements on the strength and modulus of β-type bio-titanium alloys, Mater Sci Eng A. 260; 1999. https://doi.org/10.1016/S0921-5093(98)00886-7

[7] Elias LM, Schneider SG, Schneider S, Silva HM, Malvisi F. Microstructural and mechanical characterization of biomedical Ti-Nb-Zr-(-Ta) alloys, Mater Sci Eng A. 432; 2006. https://doi.org/10.1016/j.msea.2006.06.013.

[8] Gordin DM, Gloriant T, Nemtoi Gh. Chelariu. R. Aelenei, N, Guillou A, Ansel D. Synthesis, structure and electrochemical behavior of a beta Ti-12Mo-5Ta alloy as new biomaterial, Mater Lett. 59; 2005. https://doi.org/10.1016/j.matlet.2004.09.063.

[9] Fatimah J, Al-Hasani. Evaluation of Surface Roughness and Biological Behavior of TiNb Alloys. 43; 2020.

[10] Zhang LC, Chen LY. A Review on Biomedical Titanium Alloys: Recent Progress and Prospect, Adv. Eng. Mater. 21; 2019. https://doi.org/10.1002/adem.201801215.

[11] Kaur M, Singh K. Review on titanium and titanium based alloys as biomaterials for orthopaedic applications, Mater. Sci. Eng. C. 102; 2019. https://doi.org/10.1016/j.msec.2019.04.064.

[12] Hong SH, Hwang YJ, Park SW, Park CH, Yeom JT, Park JM, Kim KB. Low-cost beta titanium cast alloys with good tensile properties developed with addition of commercial material. J. Alloy. Compd. 793; 2019. https://doi.org/10.1016/j.jallcom.2019.04.200.

[13] Sandu AV, Baltatu MS, Nabialek M, Savin A, Vizureanu P. Characterization and Mechanical Proprieties of New TiMo Alloys Used for Medical Applications, Materials (Basel, Switzerland), 12; 2019. https://doi.org/10.3390/ma12182973.

[14] Min X, Chen X, Emura S, Tsuchiya K. Mechanism of twinning-induced plasticity in β-type Ti–15Mo alloy, Scr. Mater. 69;2013. https://doi.org/10.1016/J.SCRIPTAMAT.2013.05.027

[15] Ho WF, Ju CP, Lin JHC. Structure and properties of cast binary Ti–Mo alloys. Biomaterials. 20; 1999. https://doi.org/10.1016/S0142-9612(99)00114-3.

[16] de Vasconcellos LMR, de Oliveira M.V, Graça MLA, de Vasconcellos LGO, Carvalho YR, Cairo CAA. Porous titanium scaffolds produced by powder metallurgy for biomedical applications, Materials Research. 11; 2008. https://doi.org/10.1590/s1516-14392008000300008.

[17] Rossi MC, Bayerlein DL, Gouvêa E de S, Haro Rodríguez MV, Escuder AV, Borrás VA. Evaluation of the influence of low Mg content on the mechanical and microstructural properties of β titanium alloy. J. Mater. Res. Technol. J. 10; 2021. https://doi.org/10.1016/j.jmrt.2020.12.103.

[18] Sochacka P, Miklaszewski A, Kowalski K, Jurczyk M. Influence of the Processing Method on the Properties of Ti-23 at.% Mo Alloy. Metals. 9; 2019. https://doi.org/10.3390/met9090931.

[19] Welsch G, Boyer R, Collings EW. Materials Properties Handbook: Titanium Alloys; ASM International: Materials Park, OH, USA, 1994; ISBN 978-0-87170-481-8.

[20] Cotton JD, Briggs RD, Boyer RR, Tamirisakandala S, Russo P, Shchetnikov N, Fanning JC. State of the Art in Beta Titanium Alloys for Airframe Applications. J. Met. Mater. Miner. 67; 2015. https://doi.org/10.1007/s11837-015-1442-4.

[21] Bania PJ. Beta titanium alloys and their role in the titanium industry. J. Met. Mater. Miner. 46; 1994. https://doi.org/10.1007/BF03220742.

[22] Kang N, Li Y, Lin X, Feng E, Huang W. Microstructure and tensile properties of Ti-Mo alloys manufactured via using laser powder bed fusion, J. Alloys Compd. 771; 2019. https://doi.org/10.1016/j.jallcom.2018.09.008.

[23] Louzguine-Luzgin DV. High-Strength Ti-Based Alloys Containing Fe as One of the Main Alloying Elements, Mater. Trans. 59;2018. https://doi.org/10.2320/matertrans.m2018114.

[24] Cotton JD, Briggs RD, Boyer RR, Tamirisakandala S, Russo P, Shchetnikov NC, Fanning JC. State of the Art in Beta Titanium Alloys for Airframe Applications, J. Met. Mater. Miner. 67 (2015) 1281–1303. https://doi.org/10.1007/s11837-015-1442-4.

[25] Min XH, Emura S, Nishimura T, Zhang L, Tamilselvi S, Tsuchiya K, Tsuzaki K. Microstructure, tensile deformation mode and crevice corrosion resistance in Ti-10Mo-xFe alloys, Mater. Sci. Eng. A. 527; 2010. https://doi.org/10.1016/j.msea.2010.06.016.

[26] Min X, Bai P, Emura S, Ji X, Cheng C, Jiang B, Tsuchiy K. Effect of oxygen content on deformation mode and corrosion behavior in β-type Ti–Mo alloy, Mater. Sci. Eng A.684;2017. https://doi.org/10.1016/j.msea.2016.12.062.

[27] Esteban PG, Bolzoni L, Ruiz-Navas EM, Gordo E. PM processing and characterisation of Ti–7Fe low cost titanium alloys, Powder Metall. 54;2011. https://doi.org/10.1179/174329009X457063.

[28] Hsu HC, Wu SC, Hsu SK, Li CT, Ho WF. Effects of chromium addition on structure and mechanical properties of Ti–5Mo alloy, Mater. Des. 65; 1980-2015. https://doi.org/10.1016/j.matdes.2014.09.07.

[29] Boyer R, Collings EW, Welsch G. (1994). *Materials properties handbook: Titanium alloys*. ASM International, Ohio, EEUU.

[30] Mohammed MT, Khan ZA, Siddique AN. Beta Titanium Alloys: The Lowest Elastic Modulus for Biomedical Applications: A Review. 8; 2014. https://doi.org/10.5281/zenodo.1094481.

[31] Zhao G, Li X, Petrinic N. Materials information and mechanical response of TRIP/TWIP Ti alloys, Comput Mater. 7; 2021. https://doi.org/10.1038/s41524-021-00560-2.

[32] Martins JRS, Araújo RO, Donato TAG, Arana-Chavez VE, Buzalaf MAR, Grandini CR. Influence of oxygen content and microstructure on the mechanical properties and biocompatibility of Ti–15Mo alloy used for biomedical applications, Materials. 7; 2014. https://doi.org/10.3390/ma7010232.

[33] Yan M, Qian M, Kong C, Dargusch MS. Impacts of trace carbon on the microstructure of as-sintered biomedical Ti–15Mo alloy and reassessment of the maximum carbon limit, Act. Biomat. 10; 2014. https://doi.org/10.1016/j.actbio.2013.10.034.

[34] Hsu HC, Wu SC, Hsu SK, Lin TF, Ho WF. Structure and mechanical properties of as-cast Ti–5Nb–xCr alloys, Mat.&Design. 51; 2013. https://doi.org/10.1016/j.matdes. 2013.04.001

[35] Min XH, Emura S, Nishimura T, Tsuchiya K, Tsuzaki K. Microstructure, tensile deformation mode and crevice corrosion resistance in Ti10MoXFe alloys, Mat. Sci. Eng. A. 527; 2010a). https://doi.org/10.1016/j.msea.2010.06.016.

[36] Min XH, Emura S, Sekido N, Nishimura T, Tsuchiya K, Tsuzaki K. Effects of Fe addition on tensile deformation mode and crevice corrosion resistance in Ti15Mo alloy, Mat. Sci. Eng. A. 527;2010b. https://doi.org/10.1016/j.msea.2009.12.050.

[37] Ivasishin OM, Anokhin VM, Demidik AN, Savvakin DG. Cost-effective blended elemental powder metallurgy of titanium alloys for transportation application, Key Eng. Mat. 188; 2000. https://doi.org/10.4028/www.scientific.net/KEM.188.55.

[38] Liu Y, Chen LF, Tang HP, Liu CT, Liu B, Huang BY. Design of powder metallurgy titanium alloys and composites, Mat. Sci. Eng A. 418; 2006. https://doi.org/10.1016/ j.msea.2005.10.057.

[39] O'Flynn J, Corbin SF. The influence of iron powder size on pore formation, densification and homogenization during blended elemental sintering of Ti–2.5Fe, J. Alloys Comp. 618; 2015. https://doi.org/10.1016/j.jallcom.2014.08.134.

[40] Wei WF, Liu Y, Tang HP, Huang BY. Effect of Fe addition on sintering behaviour of titanium powder, Powder Metall. 46; 2003. https://doi.org/10.1179/ 003258903225005295.

[41] Liu Y, Chen LF, Tang HP, Liu CT, Liu B, Huang BY. Design of powder metallurgy titanium alloys and composites, Mat. Sci. Eng A. 418; 2006. https://doi.org/10.1016/j.msea.2005.10.057.

[42] Ebied SM, Gepreed MA-H, Hamada A. Microstructural evolution of two binary β-titanium alloys during cold deformation, IOP Conf. Series: Mater. Sci. & Eng. 201; 2017. https://doi.org/10.1088/1757-899X/201/1/012047.

[43] Ho WF. Effect of omega phase on mechanical properties of Ti-Mo alloys for biomedical applications, J. Med. Biol. Eng. 28; 2008.

[44] Ivasishin OM, Markovsky PE, Matviychuk YV, Semiatin SL, Ward CH, Fox S. A comparative study of the mechanical properties of high-strength β-titanium alloys, J. Alloys & Comp. 457; 2008. https://doi.org/10.1016/j.jallcom.2007.03.070.

[45] Min XH, Emura S, Nishimura T, Zhang S, Tamilselvi L, Tsuchiya K, Tsuzaki K. Effects of α phase precipitation on crevice corrosion and tensile strength in Ti-15Mo alloy, Mater. Sci. Eng. A. 527; 2010c. https://doi.org/10.1016/j.msea.2009.10.033.

[46] Esteban PG, Bolzoni L, Ruiz-Navas EM, Gordo E. PM processing and characterisation of Ti–7Fe low cost titanium alloys, Powder Metall. 54; 2011. https://doi.org/10.1179/174329009X457063

[47] Hsu HC, Wu SC, Hsu SK, Li CT, Ho WF. Effects of Cr addition on structure and mechanical properties of Ti-5Mo alloy, Mat. & Design 65; 2015. https://doi.org/10.1016/ j.matdes.2014.09.077.

[48] Xu W, Lu X, Zhang B, Liu Ch, Yang S.L, Qu. X. Effects of porosity on mechanical properties and corrosion resistances of pm-fabricated porous Ti-10Mo alloy, Metals 8; 2018. https://doi.org/10.3390/met8030188.

[49] Liu Y, Wei WF, Zhou KC, Chen LF, Tang HP. Microstructures and mechanical behaviour of PM TiMo alloys, J. Cent. S. Univ. Tech. 10; 2003. https://doi.org/10.1007/ s11771-003-0043-5.